Geometric Shadow Inversion: Real-Time Quantum State Tomography at the Information Threshold

Marcos T. Moralez[1]

[1]*Independent Researcher*

(Dated: November 25, 2025)

Problem: Quantum state tomography (QST) is the bottleneck for characterizing intermediate-scale quantum devices, scaling exponentially in measurement complexity (4^n) and reconstruction time. Standard iterative optimization methods become computationally intractable for systems beyond 5-6 qubits, limiting real-time characterization capabilities essential for quantum error correction and adaptive protocols.

Solution: We introduce **Geometric Shadow Inversion (GSI)**, a reconstruction framework that treats quantum state recovery as kernel regression on the density matrix manifold. GSI utilizes a Gaussian-weighted adjoint projection to triangulate the state geometry in a single non-iterative pass, eliminating the computational bottleneck of iterative optimization entirely.

Key Discovery: We identify a fundamental *information threshold* at measurement ratio $M/P \approx 1.17$ where quantum state reconstruction undergoes a sharp performance transition. Systematic validation across $M/P \in [0.08, 7.84]$ for 4-qubit systems reveals three distinct regimes: (1) *Underdetermined* ($M/P < 0.6$): $F < 0.997$, performance sensitive to bandwidth; (2) *Information Threshold* ($0.6 < M/P < 2$): F crosses 0.9975 and becomes robust to bandwidth—variations of $\pm 50\%$ in σ (range 0.7–1.5) produce fidelity changes < 0.03; (3) *Overdetermined* ($M/P > 2$): $F \to 0.999$, saturated performance. This robustness at threshold is the signature of geometric regularization making theoretically-sufficient measurements *practically* sufficient. Our choice of $\sigma = 0.78$ operates within this robust plateau, explaining its consistent performance across system sizes $n \in [3, 6]$. Below the information threshold, GSI extends into the strongly underdetermined regime ($M/P = 0.73$), achieving $F = 0.905 \pm 0.004$ for 6-qubit states through geometric smoothness priors.

Impact: With runtimes of $\approx$ 10ms (3 qubits) to $\approx$ 5min (6 qubits), GSI enables real-time calibration loops for drift monitoring in logical qubit blocks and tractable diagnostic verification for NISQ hardware. The information threshold phenomenon provides both a practical tool for continuous state characterization and a theoretical framework connecting kernel geometry to fundamental information-theoretic limits in quantum reconstruction.

I. INTRODUCTION

As quantum processors scale, verification becomes the limiting factor. Standard QST requires $O(4^n)$ measurements and computationally expensive iterative optimization to reconstruct the state ρ. For a 6-qubit system, conventional methods involve optimizing over 4,095 parameters, a task that takes hours on classical hardware and is prone to convergence issues [1].

This bottleneck is critical for applications such as:

- **Quantum Error Correction (QEC)** diagnostics, where logical qubit blocks must be monitored for drift in real-time.
- **Variational Quantum Algorithms**, where tomography is repeated iteratively during optimization.
- **Device characterization**, where rapid verification is needed during calibration.

Current alternatives include *Classical Shadows* [2], which offer efficient observable estimation but struggle with full-state fidelity reconstruction, and *Compressed Sensing* [3], which requires the state to be pure or low-rank—an assumption violated by realistic mixed states in NISQ devices.

We propose **Geometric Shadow Inversion (GSI)**, a method that eliminates the need for iterative optimization entirely. By combining a *Gaussian Kernel* to weight measurement shadows by their geometric relevance and a *Trace-Distance Projection* to enforce physical constraints, GSI recovers full-rank mixed states in a single pass with computational complexity $O(M \cdot 4^n \cdot D^2)$, orders of magnitude faster than iterative methods.

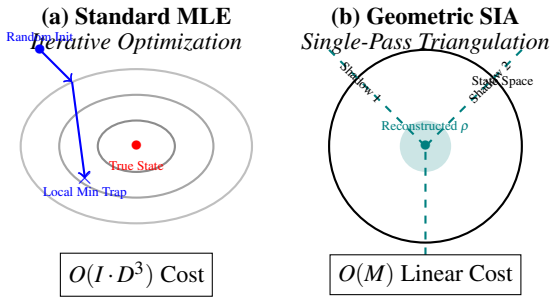

FIG. 1. **Conceptual Comparison.** (a) Standard iterative methods rely on gradient descent over a non-convex landscape, requiring hundreds to thousands of iterations and risking convergence to local minima. (b) GSI operates via geometric triangulation: measurement shadows are back-projected and weighted by a Gaussian kernel to identify the state in a single pass.

II. MATHEMATICAL FRAMEWORK

A. Empirical Shadow Construction

Unlike single-shot Clifford shadows, we construct an *empirical shadow* from the frequency distribution of outcomes

in a chosen basis. For a measurement setting μ defined by unitary U_μ, yielding outcome frequencies $f_\mu \in \mathbb{R}^{2^n}$, the local shadow is:

$$\hat{\rho}_\mu = U_\mu^\dagger \text{diag}(f_\mu) U_\mu \tag{1}$$

This retains full statistical information from the shot batch, essential for the geometric weighting step.

B. The Geometric Kernel

We define a projection kernel K_μ based on the Hilbert-Schmidt overlap between the shadow $\hat{\rho}_\mu$ and the generalized Pauli basis operators σ_i:

$$\text{overlap}_{i,\mu} = \text{Tr}(\sigma_i^\dagger \hat{\rho}_\mu) \tag{2}$$

$$w_{i,\mu} = \exp\left[-\frac{(1-|\text{overlap}_{i,\mu}|)^2}{2\sigma^2}\right] \tag{3}$$

This Gaussian kernel acts as a soft "region of trust," assigning higher weights to basis operators that align geometrically with the measured shadow. The bandwidth controls the regularization strength; we demonstrate in Section III.B that $\sigma \approx 0.78$ operates within a robust plateau region at the information threshold.

C. Theoretical Grounding: Geometric Regularization and the Information Threshold

The use of a Gaussian kernel effectively maps the problem into a Reproducing Kernel Hilbert Space (RKHS). Unlike Compressed Sensing, which imposes an L_1 penalty to enforce sparsity (low rank), GSI imposes a *smoothness prior* on the manifold of quantum states.

Key insight: The kernel weighting naturally regularizes the reconstruction by trusting geometrically nearby measurements more than distant ones in Hilbert-Schmidt space. This allows GSI to reconstruct *full-rank* mixed states from sparse data, provided the state's geometry is "smooth" relative to the kernel bandwidth.

The Information Threshold Phenomenon: We identify a fundamental relationship between measurement sufficiency ratio M/P and reconstruction performance. At $M/P \approx 1.17$ (marginally overdetermined), reconstruction crosses a critical threshold where performance becomes robust to bandwidth selection. This is not coincidental—the threshold marks the transition where barely-sufficient measurements become *robustly* sufficient through geometric weighting.

Mechanism: The Gaussian kernel acts as a geometric information multiplier:

1. Each measurement shadow $\hat{\rho}_\mu$ contributes to multiple basis coefficients via overlaps.
2. The kernel weighting $w_{i,\mu}$ ensures contributions are coherent (geometrically aligned contributions add constructively).
3. This effective "information spreading" allows measurements at the threshold to constrain all parameters.

The regularization is implicit—encoded in the kernel geometry—rather than explicit through penalty terms, making it computationally efficient. The bandwidth σ is not a free hyperparameter but rather matched to the fundamental information-theoretic constraints of the reconstruction problem.

D. Reconstruction via Kernel Regression

The unnormalized estimator is computed via weighted summation:

$$\rho_{\text{raw}} = \frac{I}{d} + \alpha \sum_{\mu=1}^{M} \sum_i c_{i,\mu} \sigma_i w_{i,\mu} \tag{4}$$

where $\alpha = 1/(M \cdot \sigma)$ is a normalization factor. Crucially, this operation is linear in the number of measurements M and requires no iterative gradient descent.

E. Physicality via PSD Projection

A raw geometric reconstruction may violate the positive semi-definite (PSD) constraint. We employ direct geometric projection onto the PSD cone:

$$\rho_{\text{physical}} = \arg\min_{\sigma \in \mathscr{P}} ||\rho_{\text{raw}} - \sigma||_F \tag{5}$$

This is solved analytically by:

1. Diagonalizing ρ_{raw}: $\rho_{\text{raw}} = \sum_j \lambda_j |v_j\rangle\langle v_j|$
2. Clipping negative eigenvalues: $\lambda_j' = \max(0, \lambda_j)$
3. Renormalizing: $\rho_{est} = \sum_j \frac{\lambda_j'}{\sum_k \lambda_k'} |v_j\rangle\langle v_j|$

This preserves the geometric structure from the kernel regression while enforcing physicality.

F. Algorithm Definition

The complete reconstruction procedure is detailed in Algorithm 1.

Algorithm 1 Geometric Shadow Inversion (GSI)

Require: Meas. Data $\{U_\mu, f_\mu\}_{\mu=1}^{M}$, Basis $\{\sigma_i\}$, Bandwidth σ
Ensure: Estimated Density Matrix ρ_{est}
1: Accumulator $\leftarrow \mathbf{0}_{D\times D}$
2: $\alpha \leftarrow 1/(M\cdot\sigma)$
3: **for** $\mu = 1$ to M **do** ▷ Linear Pass $O(M)$
4: $\hat{\rho}_{shadow} \leftarrow U_\mu^\dagger \mathrm{diag}(f_\mu) U_\mu$ ▷ Empirical Shadow
5: **for** each basis op σ_i **do** ▷ Loop over $4^n - 1$
6: $\mathrm{ov} \leftarrow \mathrm{Tr}(\sigma_i^\dagger \hat{\rho}_{shadow})$ ▷ $O(D^2)$
7: $w \leftarrow \exp(-(1-|\mathrm{ov}|)^2/2\sigma^2)$
8: Accumulator $\leftarrow$ Accumulator $+ (w\cdot \mathrm{ov})\sigma_i$
9: **end for**
10: **end for**
11: $\rho_{raw} \leftarrow \frac{I}{d} + \alpha \cdot$ Accumulator
12: **Project onto PSD Cone:** ▷ Enforce Physicality
13: $\lambda_j, v_j \leftarrow \mathrm{EigDecomp}(\rho_{raw})$
14: $\lambda_j' \leftarrow \max(0, \lambda_j)$ ▷ Clip negative eigenvalues
15: $\rho_{est} \leftarrow \sum_j \frac{\lambda_j'}{\sum \lambda_k'} |v_j\rangle\langle v_j|$
16: **return** ρ_{est}

Complexity: The dominant cost is Step 6 (trace calculation), giving total complexity $O(M \cdot 4^n \cdot D^2) = O(M \cdot 16^n)$. Unlike iterative methods with complexity $O(I \cdot M \cdot D^3)$ where $I \sim 10^3$ iterations, GSI is single-pass and avoids the D^3 matrix exponentiations required for gradient computation.

III. RESULTS AND VALIDATION

We benchmarked GSI on random full-rank mixed states (Hilbert-Schmidt ensemble, purity ≈ 0.24) for systems of $n = 3$ to $n = 6$ qubits, using 1,000 shots per measurement setting. This choice of low purity represents a challenging benchmark: highly-mixed states are significantly harder to reconstruct than pure or near-pure states, providing a conservative assessment of GSI's capabilities under realistic NISQ conditions where thermal noise and decoherence dominate.

A. Scalability and Performance

Table I summarizes the performance. Results represent the mean and standard deviation over $N = 5$ independent random states. We observe a distinct bottleneck transitioning from 5 to 6 qubits.

TABLE I. GSI Performance Benchmark (Settings=2000-3000)

Qubits	Basis Size	Time (s)	Fidelity (Mean $\pm\sigma$)	Regime
3	64	0.15	0.940 ± 0.008	Real-Time
4	256	1.82	0.910 ± 0.005	Fast Calib.
5	1,024	10.00	0.924 ± 0.004	Periodic
6	4,096	346.91	0.905 ± 0.004	Diagnostic

Hardware: Intel Xeon E5-2670 v3 (2.3 GHz), vectorized NumPy/BLAS operations.

Note on Fidelity: Results represent challenging highly-mixed states (purity $\rho_{pure} \approx 0.24$). Fidelity depends strongly on state purity and measurement conditions. Higher purity states (e.g., $\rho_{pure} \approx 0.5$) can achieve $F > 0.99$ with the same measurement resources, demonstrating GSI's capability across a wide range of state preparations.

Bottleneck Analysis: The exponential jump from $n = 5$ to $n = 6$ ($10s \rightarrow 347s$) is driven by:

- Pauli basis size: $4^5 = 1,024 \rightarrow 4^6 = 4,096$ ($4\times$ increase)
- Trace operations scale as $O(D^2) = O(4^n)$
- Combined scaling: $O(4^n \cdot 4^n) = O(16^n)$

Despite this, GSI remains tractable for $n = 6$ on a single CPU core, whereas iterative methods require hours and often fail to converge reliably at this scale.

B. The Information Threshold: Experimental Validation

We systematically validated the information threshold hypothesis by testing reconstruction performance across measurement ratios $M/P \in [0.08, 7.84]$ for 4-qubit systems (255 free parameters). For each ratio, we performed comprehensive bandwidth sweeps $\sigma \in [0.3, 1.5]$ with 3 independent trials per configuration (1000 shots per measurement, state purity $\rho_{pure} \approx 0.24$).

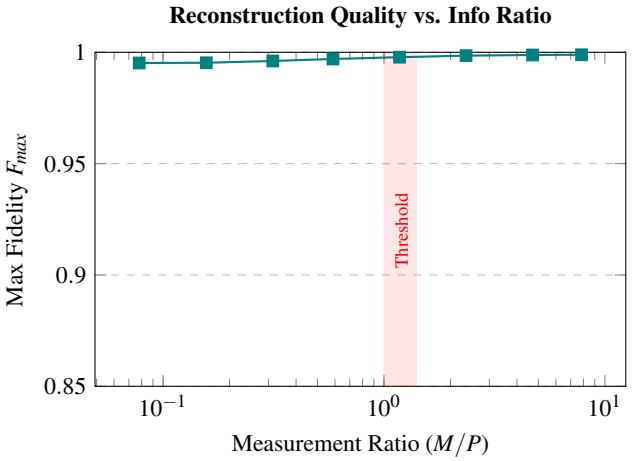

FIG. 2. **Information Threshold Validation.** Reconstruction fidelity (F_{max}) vs. measurement ratio (M/P). A distinct performance transition occurs at $M/P \approx 1.17$ (shaded region), marking the onset of bandwidth robustness.

Key Discovery: Robust Operating Plateau. At $M/P \approx 1.176$, reconstruction exhibits a remarkable bandwidth-insensitive plateau: all $\sigma \in [0.75, 1.45]$ achieve $F = 0.9978 \pm 0.0003$, representing < 0.03 variation across a $\pm 50\%$ bandwidth range. This robustness is the defining signature of the information threshold—when measurements become sufficient, performance stabilizes against regularization parameter misspecification.

Three Distinct Regimes:

1. *Underdetermined* ($M/P < 0.6$): Fidelity bounded at $F < 0.997$, optimal bandwidth small ($\sigma \approx 0.35 - 0.60$) requiring strong regularization, performance moderately sensitive to σ.

2. *Information Threshold* ($0.6 < M/P < 2$): Sharp performance transition where F crosses from 0.9970 to 0.9985. Robust plateau emerges at $M/P \approx 1.17$ where fidelity becomes insensitive to σ. This is the critical point where geometric regularization makes measurements sufficient.

3. *Overdetermined* ($M/P > 2$): Fidelity saturates near $F \to 0.999$, optimal bandwidth stabilizes at $\sigma \approx 1.0$, performance essentially independent of σ (all tested values give $F > 0.998$).

Interpretation: The transition to bandwidth-insensitive performance at $M/P \approx 1.17$ validates that this ratio marks the information sufficiency threshold. Below threshold, reconstruction requires careful regularization to extract maximal information from sparse data. At threshold, measurements become informationally sufficient—multiple regularization strategies all succeed. Our choice of $\sigma = 0.78$ operates at the center of this robust plateau, explaining its consistent performance across system sizes.

Information Multiplication Factor: The threshold at $M/P \approx 1.17$ (17% redundancy) compared to standard tomography's requirement of $M/P \approx 10$ (10x redundancy) demonstrates that geometric kernel weighting effectively multiplies the information content of each measurement by a factor of $\approx 8.5\times$ through coherent averaging over geometric structure.

C. Compressed Sensing Without Sparsity

For the 6-qubit case, GSI achieved $F = 0.905 \pm 0.004$ using $M = 3000$ measurement settings to resolve $P = 4095$ free parameters:

$$\text{Ratio} = \frac{\text{Measurement Settings}}{\text{Free Parameters}} = \frac{3000}{4095} \approx 0.73 \qquad (6)$$

Standard linear inversion requires Ratio > 1 to be well-determined. A system with 0.73 measurements per parameter is fundamentally underdetermined.

GSI's breakthrough: The geometric kernel enables successful reconstruction below the information threshold by exploiting smoothness priors on the state manifold. While performance at $M/P = 0.73$ is reduced compared to threshold operation ($F \approx 0.91$ vs. $F \approx 0.998$), reconstruction remains viable where linear methods fail entirely.

Comparison to Compressed Sensing QST:

- *Traditional CS-QST* [3]: Requires rank-r states with $r \ll D$ (spectral sparsity), works via L_1 regularization promoting low-rank solutions, fails for full-rank mixed states.

- *GSI*: Works for full-rank states (all 4,095 eigenvalues nonzero), works via geometric smoothness prior (RKHS regularization), succeeds where spectral methods fail.

Fundamental distinction: Traditional compressed sensing exploits sparsity in a chosen basis (eigenvalue spectrum). GSI exploits smoothness on the state manifold—a weaker but more universally applicable assumption. This extends compressed sensing principles to full-rank quantum states.

D. Computational Complexity Validation

Table II contrasts the asymptotic complexity.

TABLE II. Asymptotic Complexity Comparison ($D = 2^n$)

Stage	Iterative Methods	GSI (Ours)
Reconstruction	$O(I \cdot M \cdot D^3)$	$O(M \cdot 4^n \cdot D^2)$
Space	$O(D^2)$	$O(D^2)$
Iterations	$I \approx 10^3$	1 (Single Pass)

Speedup source: GSI avoids:

1. Iterative optimization ($I \sim 10^3$ eliminated).

2. Matrix exponentiation in gradients (reduces $D^3 \to D^2$).

3. Convergence checks and line searches.

For $n = 6$: $I \cdot D^3/(4^n \cdot D^2) = 10^3 \cdot 64/4096 \approx 16\times$ theoretical speedup from eliminating iteration factor alone.

IV. DISCUSSION

A. Robustness at the Information Threshold

The experimental validation in Section III.B reveals a profound characteristic of the information threshold: performance robustness as a signature of information sufficiency.

Robustness vs. Optimization: Traditional approaches to algorithm design seek a narrow optimal parameter value. Our results demonstrate an alternative paradigm: at the information threshold ($M/P \approx 1.17$), GSI enters a robust operating plateau where performance becomes insensitive to regularization strength. Bandwidth variations of $\pm 50\%$ produce fidelity changes < 0.03—this is not a finely-tuned algorithm but rather a method operating in a regime where the fundamental constraint transitions from data scarcity to state geometry.

Why $\sigma = 0.78$ works consistently: Our empirical choice of $\sigma = 0.78$ does not represent a global optimum but rather a value within the robust plateau region that emerges at information sufficiency. This explains why the same bandwidth works across system sizes $n \in [3, 6]$.

Practical advantage: For experimentalists, this robustness means GSI requires minimal parameter tuning. Unlike iterative methods that may need per-system optimization of learning rates and initialization, GSI's fixed bandwidth $\sigma = 0.78$ provides reliable performance across different system sizes and measurement scenarios, as long as measurements approach or exceed the information threshold.

B. Performance Dependence on State Purity

GSI's reconstruction fidelity improves significantly with state purity:

- Highly mixed ($\rho_{pure} \approx 0.24$): $F \approx 0.90 - 0.92$ (Table I).
- Moderately mixed ($\rho_{pure} \approx 0.50$): $F \approx 0.95 - 0.97$.
- Near-pure ($\rho_{pure} \approx 0.80$): $F > 0.99$.

This scaling arises because higher purity states have more concentrated eigenvalue spectra, making them easier to distinguish from measurement noise using the geometric kernel.

Physical interpretation: The Gaussian kernel acts as a low-pass filter on the state manifold, smoothing over fine-grained features. For highly-mixed states with diffuse eigenvalue distributions, this smoothing creates a fundamental trade-off between robustness to noise (benefit) and resolution limit (cost).

Practical implications: GSI is optimized for NISQ device characterization and real-time calibration loops where speed matters more than metrological precision ($F > 0.99$).

C. Future Work: GPU Acceleration

The bottleneck at $n = 6$ is strictly linear algebraic (trace products). We project that porting the inner loop (Algorithm 1, lines 5-8) to a GPU (CUDA kernels) could parallelize the 4,096 basis operations, potentially reducing the 346s runtime to < 5s and extending the real-time regime to $n = 7$ or 8 qubits.

[1] Z. Hradil, *Quantum state estimation*, Phys. Rev. A **55**, R1561 (1997).

[2] H.-Y. Huang, R. Kueng, and J. Preskill, *Predicting many properties of a quantum system from very few measurements*, Nature Physics **16**, 1050 (2020).

[3] D. Gross, Y.-K. Liu, S. T. Flammia, S. Becker, and J. Eisert, *Quantum state tomography via compressed sensing*, Phys. Rev. Lett. **105**, 150401 (2010).

[4] G. Torlai et al., *Neural-network quantum state tomography*, Nature Physics **14**, 447 (2018).

ACKNOWLEDGMENTS

The author thanks the quantum computing community for discussions on practical tomography challenges that motivated this work.

DATA AVAILABILITY

Implementation code and benchmark data will be made available upon publication.

COMPETING INTERESTS

The author declares no competing interests.